A General Constant Power Generation Algorithm for Photovoltaic Systems

Tafti, Hossein Dehghani; Maswood, Ali Iftekhar; Konstantinou, Georgios; Pou, Josep; Blaabjerg, Frede

2017

Tafti, H. D., Maswood, A. I., Konstantinou, G., Pou, J., & Blaabjerg, F. (2017). A General Constant Power Generation Algorithm for Photovoltaic Systems. IEEE Transactions on Power Electronics, in press.

https://hdl.handle.net/10356/83870

https://doi.org/10.1109/TPEL.2017.2724544

A General Constant Power Generation Algorithm for Photovoltaic Systems

Hossein Dehghani Tafti[1*], *Student Member, IEEE,* Ali Iftekhar Maswood[1], *Senior Member, IEEE,* Georgios Konstantinou[2], *Member, IEEE,* Josep Pou[1], *Fellow, IEEE,* Frede Blaabjerg[3], *Fellow, IEEE*

[1]School of Electrical and Electronic Engineering, Nanyang Technological University, Singapore.

[2]School of Electrical Engineering and Telecommunications, University of New South Wales, Australia.

[3]Department of Energy Technology, Aalborg University, Denmark.

[*] hossein002@e.ntu.edu.sg

Abstract

Photovoltaic power plants (PVPPs) typically operate by tracking the maximum power point in order to maximize conversion efficiency. However, with the continuous increase of installed grid-connected PVPPs, power system operators have been experiencing new challenges, like overloading, overvoltages and operation during grid voltage disturbances. Consequently, constant power generation (*CPG*) is imposed by grid codes. An algorithm for the calculation of the photovoltaic panel voltage reference, which generates a constant power from the PVPP, is introduced in this paper. The key novelty of the proposed algorithm is its applicability for both single- and two-stage PVPPs and flexibility to move the operation point to the right- or left-side of the maximum power point. Furthermore, the execution frequency of the algorithm and voltage increments between consecutive operating points are modified based on a hysteresis band controller in order to obtain fast dynamic response under transients and low power oscillation during steady-state operation. The performance of the proposed algorithm for both single- and two-stage PVPPs is examined on a 50-kVA simulation setup of these topologies. Moreover, experimental results on a 1-kVA PV system validate the effectiveness of the proposed algorithm under various operating conditions, demonstrating functionalities of the proposed *CPG* algorithm.

Index Terms

Photovoltaic systems, single- and two-stage photovoltaic power conversion, constant power generation, photovoltaic panel power-voltage curve, voltage reference calculation

I. Introduction

Current-voltage characteristics and output power of photovoltaic (PV) strings vary with changes of solar irradiance, temperature and aging. Accordingly, maximum power point tracking (MPPT) techniques are applied in most of applications in order to maximize the extracted power from a given PV system and increase the overall power conversion efficiency [1]. Several MPPT algorithms, varying in approach and complexity, have been introduced in the literature [2]–[10]. Each method has various advantages and disadvantages in different aspects like computational efficiency, speed of tracking the maximum power point, operation under partial shading and power oscillations during

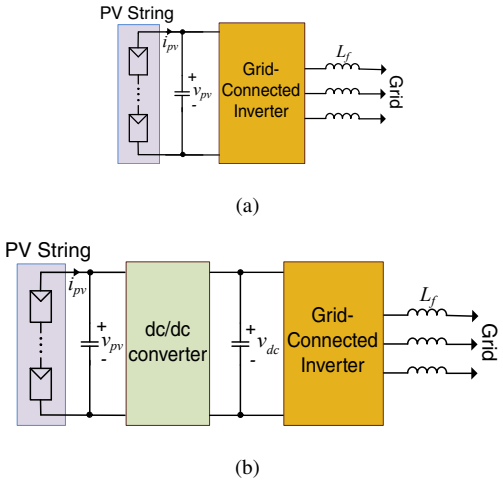

Fig. 1. Various topologies of photovoltaic power plants: (a) Single-stage power conversion structure and (b) two-stage power conversion structure.

steady-state. Among all MPPT algorithms, perturb and observe (P&O) [11]–[13] and incremental conductance (INC) [14], [15] algorithms are the most commonly used. It is shown in [16], [17] that the tracking performance of these two algorithms is similar under both static and dynamic conditions.

The focus of most of the research studies in the literature is on the extraction of maximum power from PV panels, however, there are several cases in which the control of the PV panel output active power to a certain power reference is necessary. The active power control of the PV panel is referred as constant power generation (*CPG*) in this study. One of these cases is the adaptation of PVPPs with new grid code regulations in which a constant power injection to the grid is requested. The grid codes aim to avoid the adverse effects of the high penetration of installed PVPPs in the power system, like overloading the power grid [18]. Another case is their operation during voltage sags with the requirement of simultaneous injection of active and reactive power to the grid with the aim of enhancing the voltage of the point of common coupling (PCC). By assuming that the irradiance is constant during the short duration of voltage sags, the extracted power from PV modules should be limited to a certain value in order to satisfy the inverter current limitations [19]. Therefore, a general and flexible algorithm that achieves *CPG* with fast dynamic response and low power oscillation during steady-state is essential for all different topologies of PVPPs. Two main structures of grid-connected PVPPs are single- and two-stage power conversion topologies, as depicted in Fig. 1.

Several algorithms are introduced in the literature to achieve *CPG* for different topologies of PVPPs. The basic principles of *CPG* are introduced in [18], [20]–[23] with the focus on stability issues and necessary maintenance costs of PVPPs with variable output voltage. This idea is implemented on a single-stage PVPP with the ability to control the output active power of the grid-connected inverter in order to comply with grid code requirements [24]. Moreover, a voltage reference calculation method is also introduced based on the P&O algorithm to calculate the voltage reference related to the required active power. Due to the single-stage topology, the operation point is moved to the right-side of the maximum power point (*MPP*) during the *CPG* mode. Moving the operation point to the right-side of *MPP* in [21], [24] reduces the robustness of these algorithms, because the operation point may

go beyond the open-circuit voltage of the PV panel under a fast reduction of irradiance.

To avoid the mentioned drawback, the two-stage PVPP topology is considered in [25] with the ability to achieve *CPG* operation during voltage disturbances. A multi-mode operation including MPPT, *CPG* and short-circuit current control is also implemented on the interleaved dc-dc converter. Similar *CPG* algorithms are investigated in [26], [27] based on dc-link voltage control. In these studies, the *CPG* operation is implemented by modifying the controller of the dc-dc converter to regulate the dc-bus voltage at its reference during grid disturbances. These methods need the initialization of the controllers during change of operation modes and also show slow dynamic performance.

According to the power-voltage (P-V) characteristics of the PV panel, an algorithm for the calculation of the voltage reference during *CPG* operation of the two-stage PVPP is presented and investigated in [28]–[30]. In this approach, the implementation of the *CPG* algorithm does not require any modification in the controller of the dc-dc converter. Accordingly, the calculated voltage reference from this algorithm is replaced by the voltage reference of the MPPT operation mode. As shown in [28], P&O based *CPG* control results in a faster response compared to INC algorithm under fast changes of irradiance. Moreover, in order to avoid the operation of the PV panel beyond the open-circuit voltage of the PV panel during fast changes of the irradiance, the operation point of the PV panel is moved to left-side of MPP, which limits its application only for two-stage PVPPs. Therefore, there is a need for a general algorithm for calculation of the voltage reference of the PV panel during *CPG* operation, which can be used for both single- and two-stage PVPPs during grid voltage disturbances or normal operation.

Motivated by the above, this paper proposes a new and general algorithm for the calculation of the PV panel voltage reference, which leads to generation of a constant power from the PV panel. The proposed algorithm is an adaptation of the P&O algorithm, based on the characteristics of the P-V curve of the PV panel. During the *CPG* operation, the typical MPPT algorithm is replaced with the proposed algorithm to calculate the voltage reference based on the required power reference and as a result no modification is made in the controller of the dc-dc converter. Unlike the presented studies in the literature, the proposed algorithm is flexible to move the operation point of the PV panel to the right- or left-side of the *MPP* and is also applicable in both single- or two-stage PVPPs. A hysteresis band controller is proposed to change the execution frequency of the algorithm (time-step) and voltage increments between consecutive operating points (voltage-step) in order to achieve a fast dynamic response and low power oscillation during the steady-state operation of the controller. The generality and flexibility of the proposed algorithm is evaluated using simulation and experimental validation on various PVPP topologies and different irradiance and power reference curves.

One of the key novelties of the proposed algorithm is its applicability to both single- and two-stage PVPPs. In the single-stage PVPP, the operation point during *CPG* cannot be moved to the left-side of the *MPP* in some of cases, because the dc-link voltage may become lower than the minimum dc-link voltage required for grid-connection. Therefore, for a single-stage PVPP, there is a limitation for the movement of the operation point to the left-side of the *MPP*. On the other hand, the available *CPG* algorithms, which move the operation point the right-side of the *MPP*, may experience unstable operation if the operation point goes beyond the open-circuit voltage of the PV panel due to a sudden reduction of irradiance. Therefore, the available algorithms in the literature [28]–[30], have recommended to utilize the two-stage PVPP topology in order to achieve constant power generation from the

PVPP, by moving the operation point to the left-side of *MPP* during *CPG* operation mode. Accordingly, it can be seen that the available algorithms in the literature, can only be implemented on either single- or two-stage PVPPs. However, the proposed algorithm in this paper is able to move the operation point to both right- or left-side of *MPP*. The capability of the proposed algorithm for moving the operation point to the right- or left-side of *MPP* results in its applicability to both single- and two-stage PVPPs.

The remaining of the paper is organized in the following manner. Principles of the *CPG* operation for PV strings are analyzed in Section II and the detailed implementations of the proposed *CPG* algorithm are described in Section III. The simulation results of the proposed controller on a 50-kW PVPP are presented in Section IV, while the experimental evaluation on a 1-kW PV panel is illustrated in Section V. The conclusions of the work are drawn in Section VI.

II. Constant Power Generation Principles

In this paper, the operation of the PV string is divided into two different modes:

1) Maximum power extraction mode, referred as *MPPT*, in which the maximum power (p_{mpp}) is extracted from the PV string (operating at point *MPP* in Fig. 2(a)). The conventional P&O algorithm is applied in this operation mode.
2) Constant power generation mode, named as *CPG*, in which the extracted power from the PV string is regulated to a certain power reference (P_{ref}), provided by an external controller, like the central controller of the grid-connected PVPP. The principles of the proposed algorithm for the *CPG* operation mode, which is the main contribution of this study, are presented in this section.

According to the P-V curve of the PV string (Fig. 2(a)), there are two operation points resulting in the extraction of p_{ref} from the PV string: Point *A* in the left-side of *MPP*, shown by red arrow, and Point *B* located in the right-side of *MPP*, depicted by green arrow. Each of these operation points have its advantages and disadvantages.

By moving the operation point of the PV panel to Point B in the right-side of *MPP*:

- The difference between v_b and v_{mpp} ($\mid v_{mpp} - v_b \mid$) is smaller than $\mid v_{mpp} - v_a \mid$ and therefore moving the operation point from *MPP* to Point *B* can be executed faster than to Point *A*, which results in a faster dynamic response.
- The output power of the PV panel has higher oscillation at Point *B* compared to Point *A*, because a small voltage change at this point results in a large power change.
- The operation point of the PV panel on the right-side of *MPP* may go beyond the open-circuit voltage of the PV panel under fast changes of the irradiance or temperature. This issue should be considered in the design of the *CPG* control algorithm.

By shifting the operation point of the PV panel to the Point A in the left-side of *MPP* during *CPG*:

- For small power references, it necessitates the PV string voltage to be close to the short-circuit voltage. This imposes the dc-dc converter duty cycle to be close to one, which gives poor control and large oscillation of the dc-dc converter input/output voltages and its inductor current.

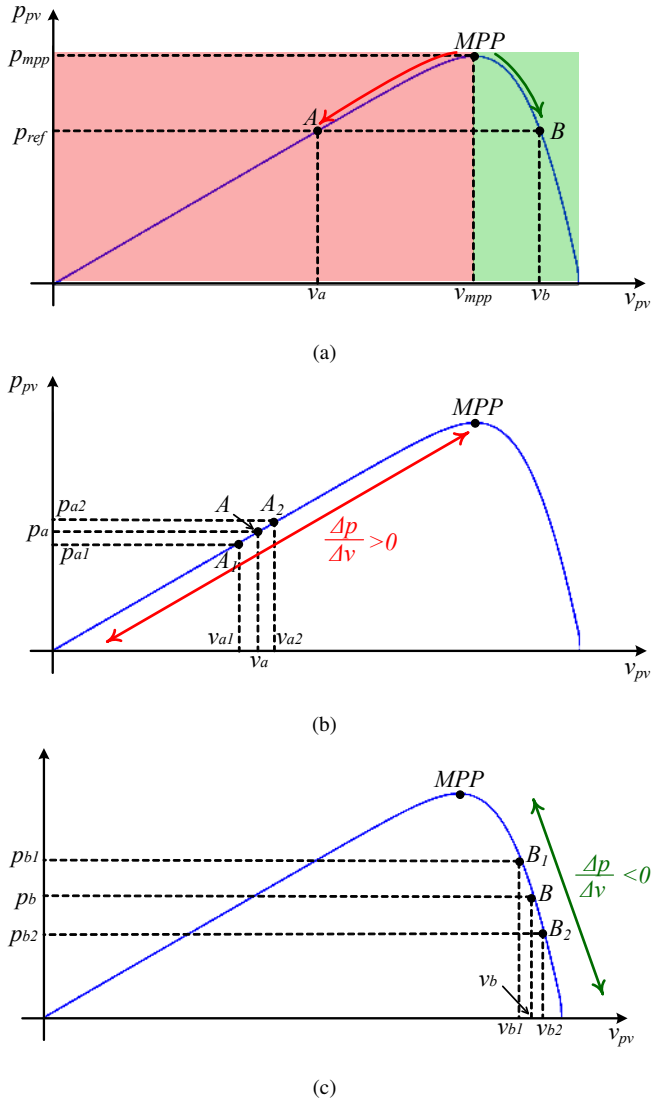

Fig. 2. Power-voltage curve of the PV string: (a) Operation at maximum power point (*MPP*), (b) operation at left-side of *MPP* and (c) operation at right-side of *MPP*.

- Because of the larger difference between V_a and V_{mpp}, the dynamic performance is slower, however the oscillation of the power at this point is smaller compared to Point *B*.

In two-stage PVPPs, the operation point during *CPG* can be moved to either right- or left-side of *MPP*, however there is a limitation in single-stage PVPPs for the movement of the operation point to the left-side of *MPP* [28], [29]. Therefore, the operation point should be moved to the right-side of *MPP* for single-stage PVPPs. By operating the single-stage PVPP in the left-side of *MPP* during *CPG*, if the dc-link voltage becomes smaller than a certain value, the grid-connected inverter is not able to produce the desired voltage for grid-connection and consequently the PVPP should be disconnected from the grid. The proposed method in this paper is flexible for moving the operation point to the right- or left-side of *MPP* and it can be used for both types of PVPPs. The operation principles of these two methods are presented in this study and each one of them can be implemented on the desired PVPP.

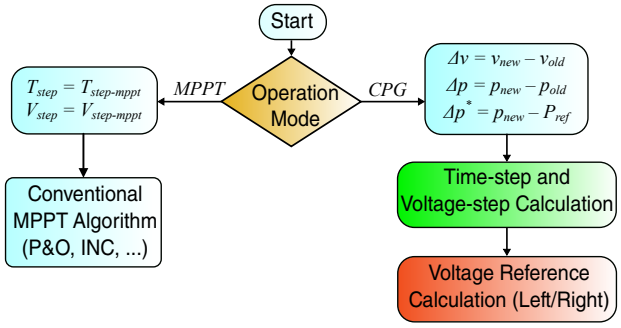

Fig. 3. Proposed voltage reference calculation strategy for both *MPPT* and *CPG* operation modes.

In order to ensure the operation of the PV string in the left- or right-side of *MPP* during *CPG* mode, the P-V curve characteristics are analyzed. Δv is defined as $\Delta v = v_{new} - v_{old}$, where v_{new} is the PV string voltage in the current time-step and v_{old} is the PV string voltage in the previous time-step. Similarly, $\Delta p = p_{new} - p_{old}$, in which p_{new} denotes the instantaneous power extracted from the PV string at the current execution time-step and is calculated by multiplying the measured instantaneous values of v_{pv} and i_{pv} (Fig. 1). The instantaneous power calculated in the previous execution time-step, is stored and used as p_{old} in the current execution time-step.

Assuming the operation at Point *A* in the current execution time-step (Fig. 2(b)), the operation point of the next time-step can be A_1 or A_2, which results in:

$$\begin{cases} \dfrac{\Delta p}{\Delta v} = \dfrac{p_{a1} - p_a}{v_{a1} - v_a} > 0 \\ \\ \dfrac{\Delta p}{\Delta v} = \dfrac{p_{a2} - p_a}{v_{a2} - v_a} > 0 \end{cases} \tag{1}$$

Consequently, $\Delta p/\Delta v$ is always positive in the left-side of *MPP*. Similarly, as presented in Fig. 2(c), moving the operation point from Point *B* to Point B_1 or B_2 in the right-side of *MPP* results in:

$$\begin{cases} \dfrac{\Delta p}{\Delta v} = \dfrac{p_{b1} - p_b}{v_{b1} - v_b} < 0 \\ \\ \dfrac{\Delta p}{\Delta v} = \dfrac{p_{b2} - p_b}{v_{b2} - v_b} < 0. \end{cases} \tag{2}$$

Therefore, $\Delta p/\Delta v$ is always negative in the right-side of *MPP*. This attribute of the P-V curve is considered in the proposed voltage reference calculation algorithm in order to ensure the operation of the PV string in the right-side of *MPP* during *CPG*.

III. Proposed Voltage Reference Calculation Algorithm

A comprehensive schematic of the proposed algorithm for the operation of PVPP during both *MPPT* or *CPG* mode is depicted in Fig. 3. The operation mode of the dc-dc converter is imposed by an external controller. If the operation mode of the PVPP is *MPPT*, the controller calculates $V_{ref} = v_{mpp}$ using an MPPT algorithm. For calculating V_{ref} during *CPG* operation, three variables including Δv, Δp and Δp^*, which is defined as $\Delta p^* = p_{new} - p_{ref}$ are calculated.

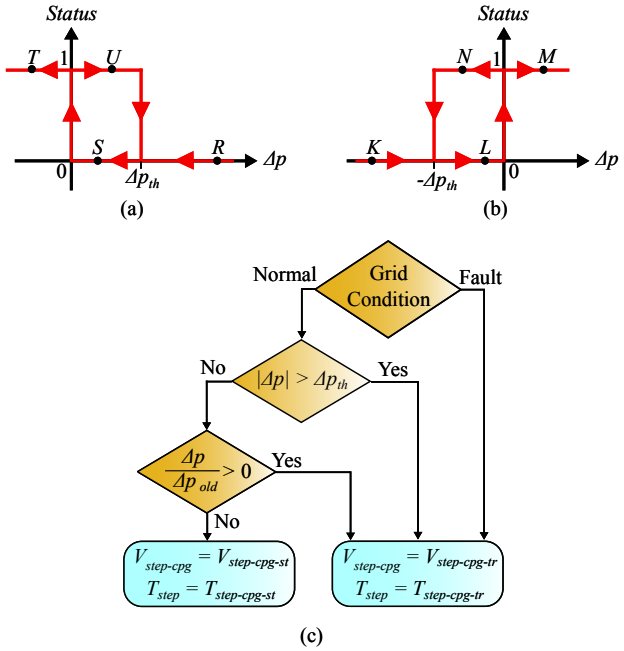

Fig. 4. Proposed voltage- and time-step calculation strategy: (a) Hysteresis controller with positive power deviation, (b) hysteresis controller with negative power deviation and (c) proposed voltage- and time-step calculation scheme.

During *MPPT* mode, the voltage calculation execution time step (T_{step}) is considered to be relatively large (e.g. $T_{step\text{-}mppt} = 0.2\,\mathrm{s}$) in order to reduce the output power oscillation during the steady-state operation. Furthermore, the voltage-step between different operating points (V_{step}) is set to be a relatively small value ($V_{step\text{-}mppt}$) in order to reduce the power oscillation during *MPPT*. However, fast performance of the controller in regulating the extracted power from PV string (p_{pv}) to a specified power reference (P_{ref}) is necessary during *CPG*. Therefore, T_{step} and V_{step} are calculated based on the proposed method using the hysteresis band controller. Afterwards, by applying the chosen V_{step} and T_{step}, the voltage reference is calculated. The detailed implementation of the proposed time- and voltage-step calculation algorithm and voltage reference calculation strategy are presented in the following subsections.

A. Proposed Time- and Voltage-Step Calculation Algorithm

It is important for the *CPG* controller to perform fast dynamic response and low power oscillation in the steady-state. Fast dynamic response is desired during fast changes of irradiance, temperature or power reference. Furthermore, during grid faults in which the active power of the PVPP should be limited to a certain value, the fast dynamic response is required for the *CPG* controller. This goal is achieved by applying different values of V_{step} and T_{step} during steady-state or transient operation modes, based on the hysteresis band controller.

The operation principle of the hysteresis band controller is depicted in Fig. 4(a) and (b). The operation is divided into two conditions based on the sign of Δp, be positive or negative. Δp_{th} is the critical (threshold) value of Δp that is used to differentiate between the steady-state and transient operation. The vertical axis, named as *Status*, refers to the operation mode of the controller. If *Status* = 1, the proper time- and voltage-step for steady-state

operation are chosen, which means $T_{step} = T_{step\text{-}cpg\text{-}st}$ and $V_{step} = V_{step\text{-}cpg\text{-}st}$. Accordingly, when *Status* = 0, T_{step} and V_{step} are set as $T_{step\text{-}cpg\text{-}tr}$ and $V_{step\text{-}cpg\text{-}tr}$, respectively, which are the chosen time- and voltage-step during the transient period.

As depicted in Fig. 4(a), if $\Delta p > \Delta p_{th}$ (operation at Point *R*), the controller operates at transient operation and *Status* = 0. By continuing the operation of the controller, Δp decreases and it becomes smaller than Δp_{th} (Point *S*). In the case that *Status* changes to 1, immediately after Δp passes Δp_{th}, the operation of the controller becomes slow and it takes long time for the controller to reach steady-state with $\Delta p \simeq 0$. Therefore, in the proposed algorithm, the *Status* remains 0 until Δp crosses zero. At $\Delta p \simeq 0$, the output power of the PV panel is close to P_{ref} and consequently, the controller should keep the operation at this point. This is achieved by changing the *Status* value to 1 at this moment, which moves the operation point to Point *T*. Afterwards, *Status* remains 1 and operation point moves between Point *T* and Point *U*. Similar procedure is implemented for negative values of Δp, as depicted in Fig. 4(b).

The detailed scheme of the proposed time- and voltage-step calculation algorithm is depicted Fig. 4(c). During grid fault condition, the controller sets T_{step} and V_{step} to $T_{step\text{-}cpg\text{-}tr}$ and $V_{step\text{-}cpg\text{-}tr}$, respectively, in order to achieve fast dynamic performance. If the grid is under normal condition and *CPG* operation is desired for the PVPP, time- and voltage-steps are calculated according to presented algorithm in this figure. If $|\Delta p| > \Delta p_{th}$, which shows the transient operation mode with *Status* = 0, as depicted in Fig. 4(a) and (b), $T_{step\text{-}cpg\text{-}tr}$ and $V_{step\text{-}cpg\text{-}tr}$ are chosen as time- and voltage-step. If $|\Delta p| < \Delta p_{th}$, *Status* can be either 0 or 1, based on the sign of Δp in the current and previous calculation-step, referred as Δp_{old}. For instance, in Fig. 4(a), if the operation point is shifted from Point *R* to Point *S* in the current calculation-step, $\Delta p/\Delta p_{old} > 0$ and *Status* is equal to 0, which sets $T_{step\text{-}cpg\text{-}tr}$ and $V_{step\text{-}cpg\text{-}tr}$ as time- and voltage-step. After the moment that Δp crosses 0, $\Delta p/\Delta p_{old} < 0$ and consequently *Status* is changed to 1 and $T_{step\text{-}cpg\text{-}st}$ and $V_{step\text{-}cpg\text{-}st}$ are selected. A similar concept can also be applied in Fig. 4(b) for negative values of Δp. The selected time- and voltage-step in this stage are considered in the proposed algorithm for calculation of the voltage reference during *CPG*.

The selection of $T_{step\text{-}cpg\text{-}tr}$, $T_{step\text{-}cpg\text{-}st}$ depends on the structure and nominal power of the PVPP. It also relies on the dynamic performance of the controller. The main criteria in the selection of these values is that, the power of the PV panel should be able to follow the change of the voltage reference in the subsequent calculation steps. It is recommended to use a transient time-step ($T_{step\text{-}cpg\text{-}tr}$) of at least ten times smaller than $T_{step\text{-}cpg\text{-}st}$ in the proposed algorithm in order to achieve fast transient response. Furthermore, $T_{step\text{-}cpg\text{-}st}$ can be considered equal to $T_{step\text{-}mppt}$. The dynamic performance of the controller in the two-stage PVPP is faster than the single-stage PVPP, thereby a smaller time-step can be considered for the two-stage PVPP during the *CPG* operation.

In addition to the above considerations, the operation point of the PV panel, being in the right- or left-side of *MPP*, should also be taken into consideration for the selection of $V_{step\text{-}cpg\text{-}tr}$ and $V_{step\text{-}cpg\text{-}st}$. By operation in the right-side of *MPP*, the voltage difference between v_{mpp} and v_b (in Fig. 2(a)) is small and therefore a relatively small $V_{step\text{-}cpg\text{-}tr}$ can result in the fast response. However, a larger $V_{step\text{-}cpg\text{-}tr}$ is required for the operation in the left-side of *MPP*, due to the relatively large voltage difference between v_{mpp} and v_a in Fig. 2(a). Furthermore, the power oscillation in the right-side of *MPP* is larger than the left-side of *MPP*, therefore a smaller $V_{step\text{-}cpg\text{-}st}$ shall

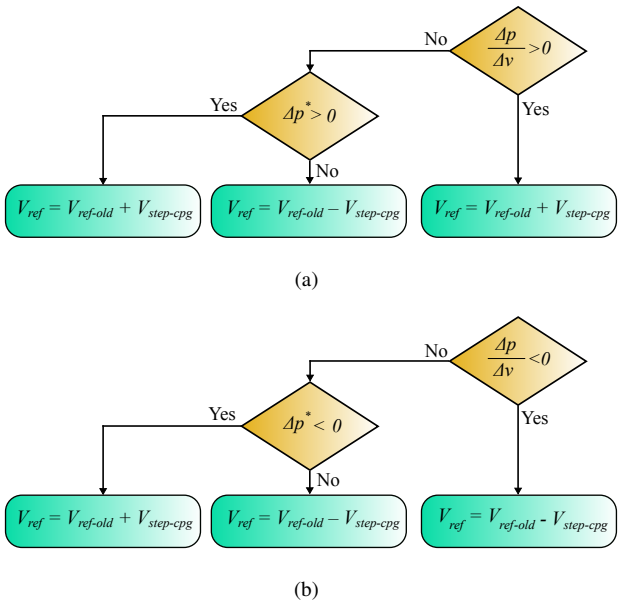

Fig. 5. Proposed voltage reference calculation strategy: (a) voltage reference calculation at right-side of *MPP* and (b) voltage reference calculation at left-side of *MPP*.

be applied for the operation on the right-side of *MPP* compared to the operation on the left-side of *MPP*.

The selection of Δp_{th} mainly depends on the nominal power of the PV string. Δp_{th} is the threshold power, which is used to differentiate between the steady-state and transient operation of the PV string during *CPG*. By selecting a relatively large value for Δp_{th}, the proposed algorithm remains in the steady-state operation mode for larger deviations of the extracted power and reference power. In this case, the steady-state error of the system becomes larger. The choice of a relatively small value for Δp_{th} results into a fast transient response of the proposed controller, however it also increases the output power oscillations of the PV string. Therefore, the selection of a reasonable value for Δp_{th} is necessary to achieve desirable performance from the proposed algorithm. Since the proposed algorithm is based on the the P&O algorithm, the available algorithms in the literature for the optimized operation of the P&O algorithm can be implemented for the adaptive selection of Δp_{th}, $T_{step\text{-}cpg\text{-}tr}$ and $V_{step\text{-}cpg\text{-}tr}$ [31]–[34].

B. Proposed Voltage Reference Calculation Algorithm

The schematic of the proposed algorithm for the calculation of the voltage reference during *CPG* operation, with the movement to left- or right-side of *MPP* is presented in Fig. 5. It should be noted that at any time only one of these methods is applied during the *CPG* operation. The detailed implementation of these methods is presented in this section.

Proposed voltage reference calculation algorithm in right-side of MPP: At the start of *CPG*, the current operation point of the PV string is determined by calculating $\Delta p/\Delta v$. If the current operating point is in the left-side of *MPP*, the voltage reference in the next execution step is increased as $V_{ref} = V_{ref\text{-}old} + V_{step\text{-}cpg}$. The relatively large amount of $V_{step\text{-}rp\text{-}tr}$, which is assigned by the controller, results in a fast movement of the

operation point to the right-side of *MPP*. After ensuring that the operation point of PV string is in the right-side of *MPP*, the proposed algorithm determines the voltage reference, related to P_{ref} by calculating Δp^*. Positive Δp^* shows that the output power is larger than P_{ref}, hence V_{ref} should be increased in the next time step, to reduce the output power (Fig. 2(c)). Similarly, for negative Δp^*, the voltage reference of the next execution step should be decreased ($V_{ref} = V_{ref\text{-}old} - V_{step\text{-}cpg}$) in order to increase the output power.

Proposed voltage reference calculation algorithm in left-side of MPP: Similar to the mentioned algorithm, after determining the current operation point of the PV string by calculating $\Delta p/\Delta v$, if the operation point is in the right-side of *MPP*, it is moved to the left-side of *MPP* by decreasing the voltage reference in the next calculation step. subsequently, the voltage reference is calculated by comparing the output power of the PV panel and P_{ref} and if Δp^* is positive/negative, the voltage reference is decreased/increased, as depicted in Fig. 5(b).

In the proposed voltage reference calculation algorithm, the main concerns regarding the operation of PV string during *CPG* are addressed as follows:

Remark 1: In order to achieve fast response, $V_{step\text{-}cpg}$ which is the voltage reference increment in each execution step, should be relatively large during the transient period. This is set to $V_{step\text{-}cpg\text{-}tr}$ during the transient period of *CPG*, which results in the fast movement of v_{ref} from v_{mpp} to v_a or v_b (Fig. 2(a)). The transient period of *CPG* is determined by using the hysteresis band controller as shown in Fig. 4(c). This transient period occurs at the start of *CPG* or fast changes of irradiance, temperature or power reference, however it can also take place during grid faults. These step changes result in quick deviation of p_{pv} and hence $T_{step\text{-}cpg} = T_{step\text{-}cpg\text{-}tr}$ and $V_{step\text{-}cpg} = V_{step\text{-}cpg\text{-}tr}$.

Remark 2: By operating at Point *A* or *B*, a small modification of the voltage reference produces a relatively large change of p_{pv}. In this study, the oscillation of p_{pv} during the steady-state of *CPG*, determined by the proposed hysteresis band controller, is reduced by imposing a relatively small value for $V_{step\text{-}cpg}$, equal to $V_{step\text{-}cpg\text{-}st}$.

Remark 3: If the required power reference is greater than the maximum available power from the PV string during *CPG*, the proposed algorithm is able to calculate the voltage of maximum power point. Assuming that the movement of operation point to the right- side of *MPP* is chosen as the *CPG* control method, at the start of *CPG*, the proposed algorithm moves the operation point to the right-side of *MPP* by increasing V_{ref}. After moving the operation point to the right-side of *MPP*, the proposed algorithm calculates Δp^* and since it is negative, v_{ref} is reduced for the next execution time step, which, as a result brings the operation point to the left-side of *MPP* again. This operation will be repeated in this condition and hence the operation point oscillates around *MPP* resulting in the extraction of the maximum available power from the PV string. Since the parameters of the proposed algorithm are optimally selected for the *CPG* operation, not for the *MPPT* operation, the proposed algorithm extracts the maximum power from the PV string under such condition. However, the output power oscillations are relatively large.

Remark 4: One of the reasons that the available algorithms in the literature move the operation point only to the left-side of *MPP* is that by moving the operation point to right-side of *MPP*, it may go beyond the open-circuit voltage on the PV string as a result of a sudden change of irradiance or temperature. However, the proposed algorithm for moving the operation point to right-side of *MPP* in this paper, can regulate the power under such

condition. As depicted in Fig. 5(a), if the operation point is in right-side of *MPP* and the power becomes smaller than P_{ref} as a result of the sudden change of irradiance or temperature, V_{ref} reduces in the subsequent steps, which moves the operation point lower than the open-circuit voltage of the PV panel.

Remark 5: The selection of the operation region of the PV panel, to be in the right- or left-side of *MPP*, is predetermined by an external controller. The proposed algorithm in this paper, calculates the PV string voltage reference based on the chosen operation region and the required power reference from the external controller. As mentioned in Section II, the operation at the right- or left-side of *MPP* has various advantages and disadvantages and accordingly, a novel algorithm can be developed, as a future work of this study, which dynamically decides the operation region based on the real time parameters of the system in order to achieve a better performance.

IV. Simulation Results

Both single- and two-stage PVPP topologies (Fig. 1) are modeled and developed using Matlab/Simulink© and the PLECS toolbox. The PV panels are modeled using the SHARP NU-U235F1 model. Each PV panel produces the maximum power of $235\,\mathrm{W}$ ($30\,\mathrm{V}$ and $7.84\,\mathrm{A}$) at $25^{\circ}\mathrm{C}$ temperature and $1\,\mathrm{kW/m^2}$ irradiance. The main system parameters are listed in Table I. The selection of voltage- and time-step are based on the criteria mentioned in Section III.

The schematic of the control algorithm, which can be implemented in both single- and two-stage PVPPs, is illustrated in Fig. 6. The operation mode and power reference are set by an external controller, like the central controller of the grid-connected PVPP. Furthermore, the operation region of the PV panel (operation in the right- or left-side of *MPP*) is also predetermined in the central controller. The operation mode is set based on the implemented fault detection and protection algorithm in the central controller. The PV string voltage reference is calculated through the proposed voltage reference calculation algorithm. Subsequently, V_{ref} is fed into the power converter controller, being the dc-dc converter in the two-stage PVPP or the grid-connected inverter in the single-stage PVPP. It should be noted that since the calculated V_{ref} using the proposed voltage reference calculation algorithm results in the regulation of the extracted power to P_{ref}, no additional controller or modifications of the dc-dc converter controller are required for the operation during *CPG* and the same controller as *MPPT* can be applied.

Although the main focus of this paper is for grid-connected PVPPs, the proposed algorithm can also be implemented on stand-alone PVPPs. In the two-stage PVPP, the proposed algorithm is implemented on the dc-dc converter and based on the inverter control algorithm, the PVPP can be utilized as stand-alone or grid-connected mode. In the single-stage PVPP, the proposed algorithm calculates the voltage reference in the outer loop of the controller, while the inner loop of the controller can be implemented as voltage controller for stand-alone PVPP or current controller for the grid-connected inverter.

In order to evaluate the generality of the proposed *CPG* algorithm, three different cases are investigated: 1) two-stage PVPP with the movement of the operation point to the right-side of *MPP*, 2) two-stage PVPP with the movement of operation point to the left-side of *MPP* and 3) single-stage PVPP with the movement of operation point to the right-side of *MPP*. Furthermore, two test scenarios are implemented in each of these three cases. In test scenario one, the performance of the proposed *CPG* algorithm under changes of irradiance is investigated, while the

TABLE I

SIMULATION PARAMETERS OF THE PHOTOVOLTAIC SYSTEM

Parameter	Symbol	Two-stage case study values	Single-stage case study values
PVPP nominal power	P	50 kW	50 kW
PV panel maximum power	p_{mpp}	235 W	235 W
PV panel maximum power point voltage	v_{mpp}	30 V	30 V
PV panel maximum power point current	i_{mpp}	7.84 A	7.84 A
Number of parallel-connected PV panels in the PV string	N_p	15	9
Number of series-connected PV panels in the PV string	N_s	15	25
PV panel filling factor	FF	0.72	0.72
dc-bus voltage	v_{dc}	770 V	770 V $(= v_{pv})$
Grid voltage	v_{pcc}	430 V_{rms}	430 V_{rms}
PV panel capacitor	C_{pv}	5 mF	5 mF
MPPT mode time-step	$T_{step\text{-}mppt}$	0.1 s	0.1 s
Steady-state *CPG* mode time-step	$T_{step\text{-}cpg\text{-}st}$	0.1 s	0.15 s
Transient *CPG* mode time-step	$T_{step\text{-}cpg\text{-}tr}$	0.002 s	0.05 s
MPPT mode voltage-step	$V_{step\text{-}mppt}$	5 V	5 V
Steady-state *CPG* mode voltage-step	$V_{step\text{-}cpg\text{-}st}$	Right-side: 1 V Left-side: 6 V	Right-side: 1 V Left-side: 6 V
Transient *CPG* mode voltage-step	$V_{step\text{-}cpg\text{-}tr}$	Right-side: 3 V Left-side: 8 V	Right-side: 3 V Left-side: 8 V
Threshold power	Δp_{th}	8 kW	8 kW

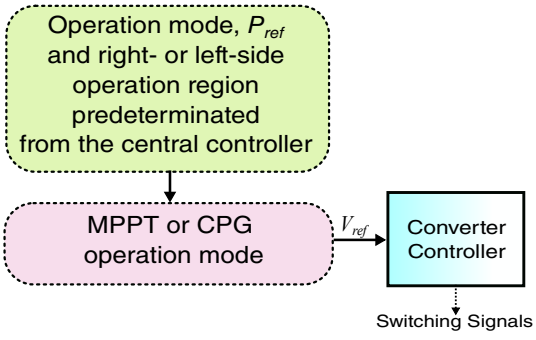

Fig. 6. Control diagram of the single- and two-stage PVPP topologies.

power reference is constant. The evaluation results for this test scenario for the three mentioned cases are presented in Cases I, II and III. In scenario two, the power reference is changed, while the transition from *MPPT* to *CPG* is also considered. The evaluation results for the second test scenario are demonstrated in Cases IV, V and VI.

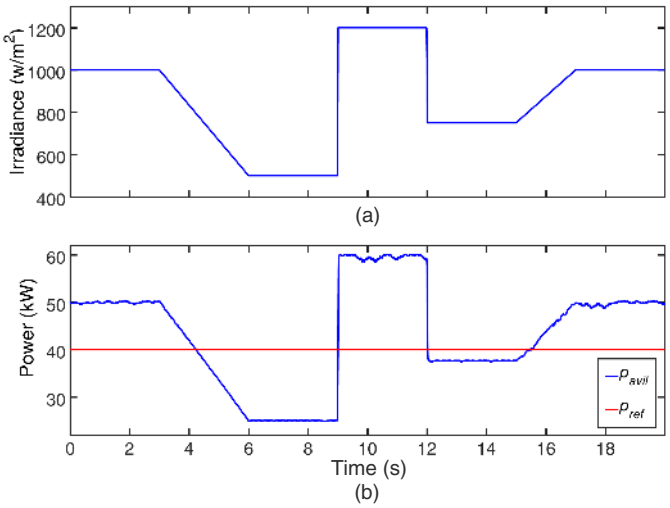

Fig. 7. Simulation results, test scenario one. (a) Implemented irradiance profile and (b) available power from the PV module at *MPP*.

The implemented irradiance profile for the first test scenario is presented in Fig. 7(a). Different types of irradiance changes, including step/ramp increase/decrease are considered in order to demonstrate the performance of the proposed algorithm under various conditions including a worst case step-change of the irradiance. Accordingly, the maximum available power from the PV panel under *MPPT* operation is illustrated in Fig. 7(b). As expected, the available power when $Irr = 1\,\mathrm{kW/m^2}$ equals to $50\,\mathrm{kW}$, while it is smaller for lower irradiance amounts and it is larger for higher amounts of irradiance. The required power reference in this test scenario is $40\,\mathrm{kW}$, and as depicted in Fig. 7(b), there are several instances that the available power from the PV panel is smaller than the required power reference.

Case I: This case demonstrates the performance of the proposed *CPG* algorithm on the two-stage PVPP with the movement of the operation point to the left-side of *MPP* and results are presented in Fig. 8. Before $t = 3\,\mathrm{s}$, $Irr = 1\ \mathrm{kW/m^2}$ and the voltage reference is regulated at $310\,\mathrm{V}$ through the proposed algorithm, which keeps the operation point of the PV panel at Point *A*, as depicted in Fig. 8(c). During this period, the time-step is equal to $0.1\,\mathrm{s}$ and the voltage-step is set to $6\,\mathrm{V}$; consequently, the output power of the PV panel experiences small power oscillation, as shown in Fig. 8(b). The irradiance decreases linearly between $t = 3\,\mathrm{s}$ and $t = 6\,\mathrm{s}$, as illustrated in Fig. 7(a). However, before $t = 4\,\mathrm{s}$, the available power is larger than P_{ref} and therefore, p_{pv} is regulated at $40\ \mathrm{kW}$ by increasing v_{pv}. It can be seen that during this transient period, small time-step and large voltage-step is used which results in the fast dynamic performance of the proposed *CPG* algorithm. Between $t = 6\,\mathrm{s}$ and $t = 9\,\mathrm{s}$, the PV string operates at Point *B*, which is its maximum power point at $Irr = 0.5\,\mathrm{kW/m^2}$, because the available power is smaller than the required power. There is a step increase of irradiance at $t = 9\,\mathrm{s}$ to $Irr = 1.2\,\mathrm{kW/m^2}$, which as a result the operation point is quickly moved to Point *C* in Fig. 8(c) with a decrease of the voltage to $v_{pv} = 250\,\mathrm{V}$. Similarly, a step decrease in the irradiance occurs at $t = 12\,\mathrm{s}$ to $Irr = 0.75\,\mathrm{kW/m^2}$ that moves the operation point to *D*. At this point, p_{pv} is approximately equal to $38\,\mathrm{kW}$, that is the maximum available power of the PV string under such irradiance. Finally, as a result of the linear increase of the irradiance, the operation point of the PV

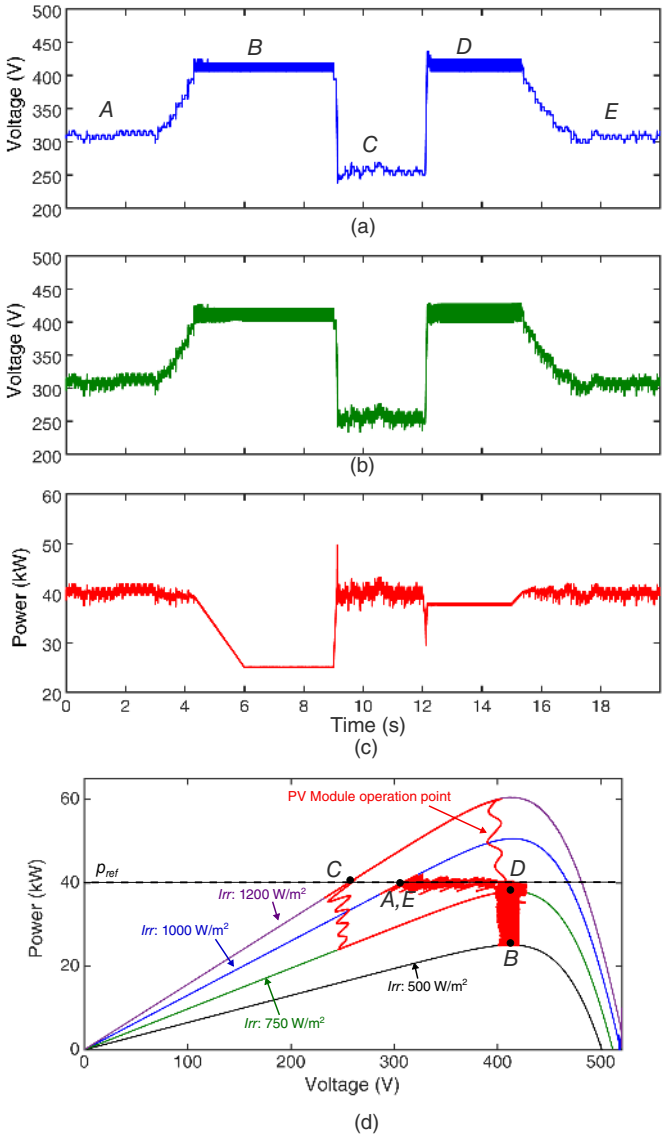

Fig. 8. Simulation results, test scenario one. *Case I*: Constant power generation of the PV module in the two-stage topology with the movement of the voltage reference to the left-side of *MPP*: (a) Voltage reference (v_{ref}), (b) PV voltage (v_{pv}), (c) extracted power from the PV module (p_{pv}) and (d) operation point of the PV module.

panel moves to Point *E*, which is the same operation point as *A*. The power oscillations during the steady-state operation of the controller are approximately $1\,\mathrm{kW}$, which indicates a tracking error of around $\pm 1\%$.

Case II: This case study examines the performance of the proposed *CPG* algorithm for the movement of the operation point to the right-side of *MPP* in the two-stage PVPP and results are depicted in Fig. 9. The same irradiance profile as Fig. 7(a) is considered in this study with $P_{ref} = 40\ \mathrm{kW}$. Before $t = 3\,\mathrm{s}$, the PV strings operates at Point *A* in Fig. 7(c) with $v_{pv} = 470\,\mathrm{V}$. Due to the decrease of irradiance after this moment, the operation point is moved to Point *B* that is the maximum power point of the PV string at $Irr = 0.5\,\mathrm{kW/m^2}$. A similar process as *Case I* is performed in this case study as well. It can be seen that the output power of the PV string is kept

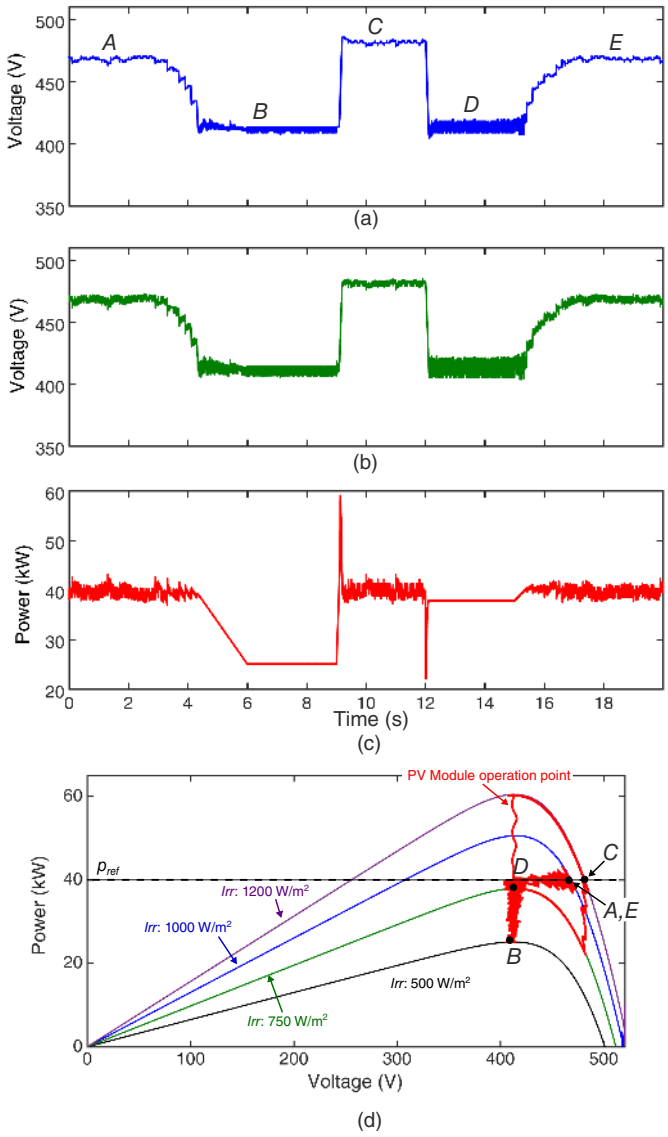

Fig. 9. Simulation results, test scenario one. *Case II*: Constant power generation of the PV module in the two-stage topology with the movement of the voltage reference to the right-side of *MPP*: (a) Voltage reference (v_{ref}), (b) PV voltage (v_{pv}), (c) extracted power from the PV module (p_{pv}) and (d) operation point of the PV module.

at 40 kW during all times, even during a sudden step change of the irradiance. Furthermore, at instances that the maximum available power is smaller than P_{ref}, the PV panel operates at *MPP*.

Case III: The operation of the proposed *CPG* algorithm with the movement of the operation point to right-side of *MPP* is examined under the irradiance profile shown in Fig. 7(a), for a single-stage PVPP with grid-connected inverter and results are depicted in Fig. 10. In this case study, the number of series-connected PV panels in the PV string is increased to 25 in order to achieve the required dc-link voltage for grid-connection. Under $Irr = 1\,\mathrm{kW/m^2}$ (before $t = 3\,\mathrm{s}$) the proposed algorithm regulates the dc-link voltage to $850\,\mathrm{V}$ (Point *A* in Fig. 10(c)). Subsequently, the operation point is moved to Point *B*, which is the maximum power point of the PV panel $Irr = 0.5\,\mathrm{kW/m^2}$ and

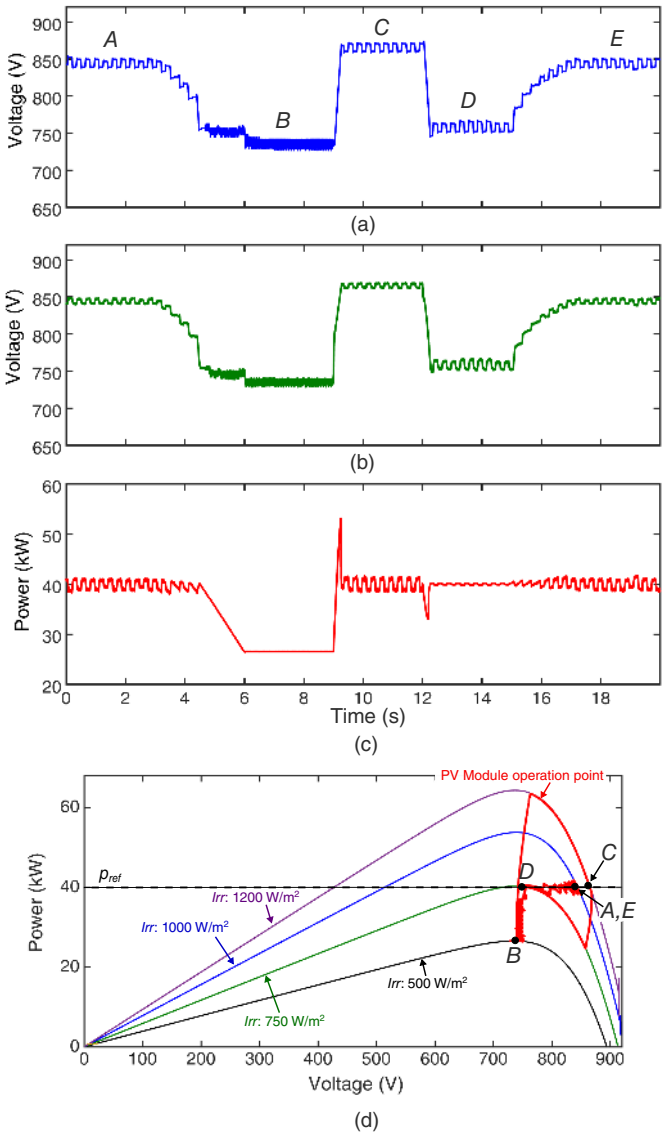

Fig. 10. Simulation results, test scenario one. *Case III*: Constant power generation of the PV module in the single-stage topology with the movement of the voltage reference to the right-side of *MPP*: (a) Voltage reference (v_{ref}), (b) PV voltage (v_{pv}), (c) extracted power from the PV module (p_{pv}) and (d) operation point of the PV module.

power of approximately 25 kW. The test scenario continues similar to *Case II* and the presented results demonstrate the capability of the proposed *CPG* algorithm in regulating the output power of the single-stage PVPP to the required power reference.

Cases IV, V and VI: In test scenario two, the performance of the proposed algorithm under three severe operation conditions is demonstrated in these case studies: 1) Change of the operation mode from *MPPT* to *CPG*, 2) step change of the power reference and 3) step decrease of the irradiation which moves the operation point beyond the open-circuit voltage of the PV string. These test scenarios are performed on the presented PVPP topologies and the results are illustrated in Figs. 11, 12 and 13. Prior to $t = 3\,\mathrm{s}$, the PVPP operates at *MPPT* and the maximum

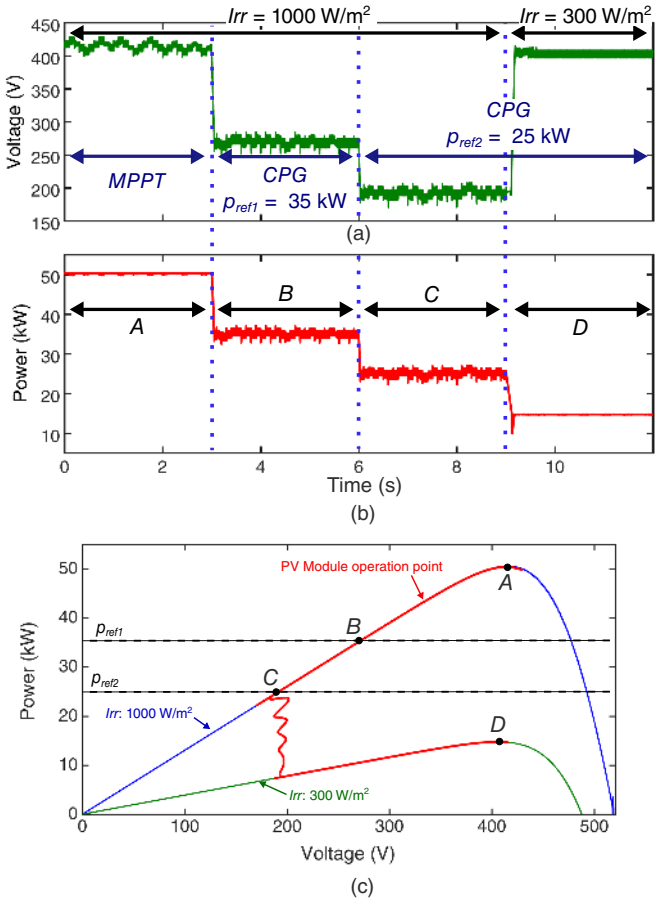

Fig. 11. Simulation results, test scenario two. *Case IV*: Constant power generation of the PV module in the two-stage topology with the movement of the voltage reference to the left-side of *MPP*: (a) Irradiance, (b) PV voltage (v_{pv}), (c) extracted power from the PV module (p_{pv}) and (d) operation point of the PV module.

available power of the PV string ($50\,\mathrm{kW}$) is extracted in all the three cases. At $t = 3\,\mathrm{s}$, the operation mode is change to *CPG* from the PVPP central controller with $P_{ref} = 35\,\mathrm{kW}$ and therefore, the proposed *CPG* algorithm quickly regulates the PV string power to the required power reference at Point *B* in all of the three cases. The power reference is decreased to $P_{ref} = 25\,\mathrm{kW}$ at $t = 6\,\mathrm{s}$. Consequently, the proposed algorithm increases/decreases the voltage reference in the right-/left-side of *MPP* to Point *C* to adjust the PV panel power with its reference value.

One of the interesting features of the proposed algorithm is its robustness for the operation in the right-side of *MPP*, when its operation point goes beyond the open-circuit voltage of the PV panel. At $t = 9\,\mathrm{s}$, a sudden decrease of the irradiance from $Irr = 1\,\mathrm{kW/m^2}$ to $Irr = 0.3\,\mathrm{kW/m^2}$ is simulated. It can be seen from Fig. 12(c) and 13(c) that the PV panel voltage is equal to $495\,\mathrm{V}$ and $883\,\mathrm{V}$ before this moment, for the two- and single-stage PVPP respectively. Due to the step reduction of the irradiance, these voltages are beyond the open-circuit voltage of the PV panel under such irradiation, which are $486\,\mathrm{V}$ and $868\,\mathrm{V}$, respectively. The proposed algorithm decreases the voltage reference under such condition and consequently brings the operation point inside the P-V curve range of the PV panel. Because the maximum available power of the PV string under this condition is smaller than P_{ref},

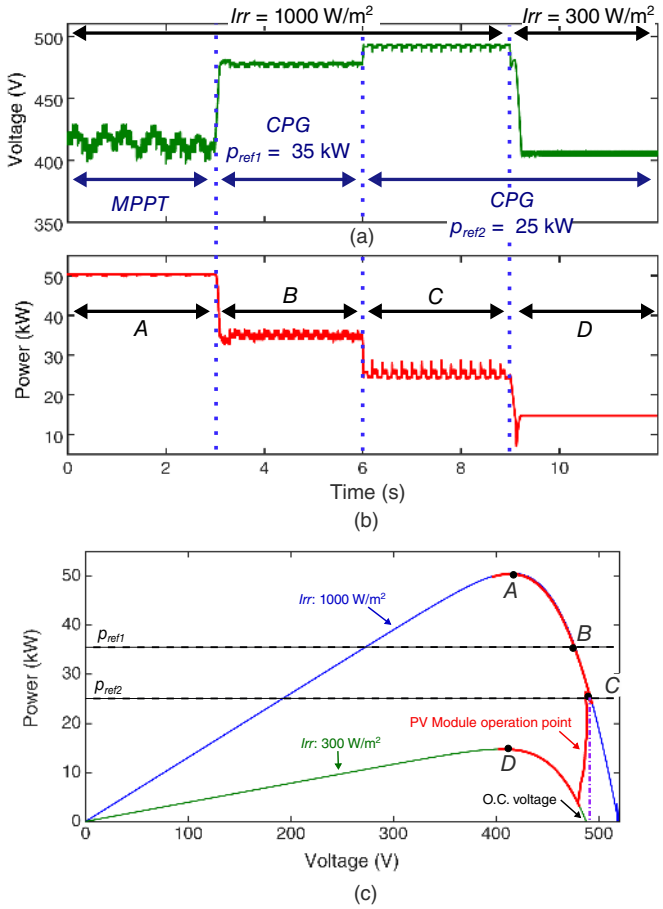

Fig. 12. Simulation results, test scenario two. *Case V*: Constant power generation of the PV module in the two-stage topology with the movement of the voltage reference to the right-side of *MPP*: (a) PV voltage (v_{pv}), (b) extracted power from the PV module (p_{pv}) and (c) operation point of the PV module.

the algorithm adjusts v_{pv}, to v_{mpp} during this period.

Simulation results demonstrate the generality of the proposed *CPG* algorithm for different types of PVPPs with the flexibility to move the operation point of the PV panel to the right- or left-side of *MPP*. Furthermore the robustness of the proposed algorithm in regulating the PV panel power under step change of irradiance and power reference is demonstrated under various operation conditions.

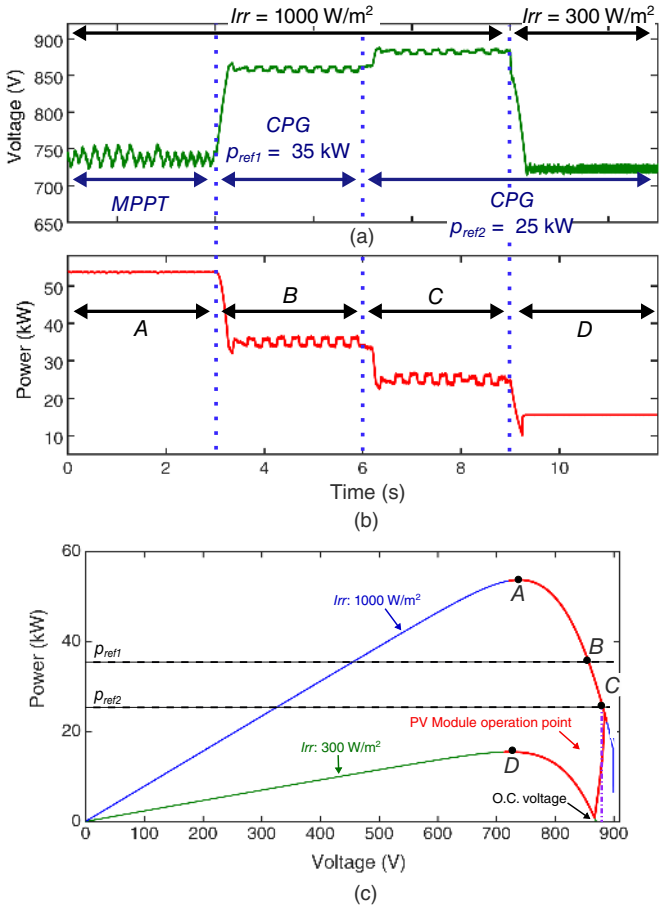

Fig. 13. Simulation results, test scenario two. *Case VI*: Constant power generation of the PV module connected in the single-stage topology with the movement of the voltage reference to the right-side of *MPP*: (a) PV voltage (v_{pv}), (b) PV power (p_{pv}) and (c) operation point of the PV module.

V. Experimental Evaluation

The operation and performance of the proposed algorithm are demonstrated experimentally using a dc-dc boost converter setup (Fig. 14) based on the CREE C2M0080120D SiC Power MOSFET. The complete parameters of the experimental setup are given in Table II and the circuit diagram of the experimental setup is shown in Fig. 14(b). The PV side is emulated using an ETS600/8 Terra SAS photovoltaic simulator and the V-I characteristics are given in Table II. The dc-side voltage is regulated with a Sorensen SGI 400-38 dc power supply in parallel with a resistor (R_l) as in practical applications it would be controlled by the inverter-side dc-voltage control. The schematic of the implemented controller is the same as the presented control strategy for simulation evaluation, shown in Fig. 6(a). The proposed controller and protection functions of the converter are implemented in a dSPACE 1006 platform.

Two different cases are experimentally tested in order to verify the operation of the controller under different situations.

Case I: This case demonstrates the performance of the proposed algorithm under direct changes in the power reference (P_{ref}) with regards to other control objectives. The irradiance and temperature are assumed to remain

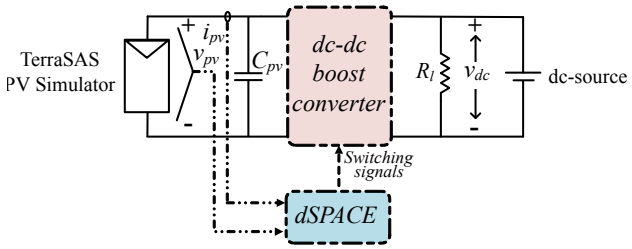

(a)

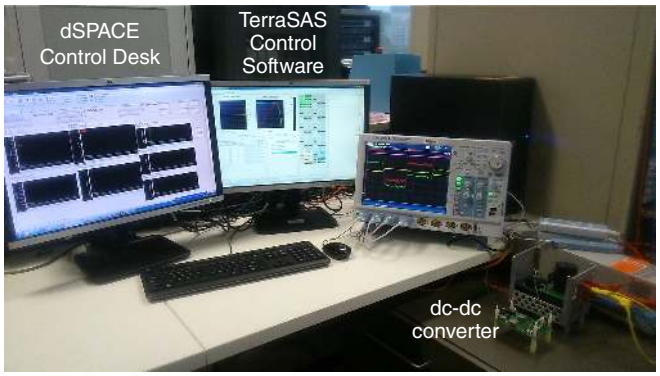

(b)

Fig. 14. Experimental verification. (a) Schematic diagram of the dc-dc converter test system and (b) setup of the experiment.

TABLE II

PARAMETERS OF THE EXPERIMENTAL SETUP

Parameter	Symbol	Value
PV panel maximum power	p_{mpp}	1 kW
PV panel maximum power point voltage	v_{mpp}	137 V
PV panel maximum power point current	i_{mpp}	7.5 A
PV panel filling factor	FF	0.77
dc-bus voltage	v_{dc}	250 V
PV panel capacitor	C_{pv}	200 μF
dc/dc converter switching frequency	f_{sw}	50 kHz
MPPT mode calculation time-step	$T_{step\text{-}mppt}$	0.2 s
CPG mode calculation time-step	$T_{step\text{-}cpg}$	0.02 s
MPPT mode voltage-step	$V_{step\text{-}mppt}$	0.5 V
Steady-state *CPG* mode voltage-step	$V_{step\text{-}cpg\text{-}st}$	0.35 V
Transient *CPG* mode voltage-step	$V_{step\text{-}cpg\text{-}tr}$	3.5 V
Threshold power	Δp_{th}	80 W

constant for the duration of the event and the results are shown in Fig. 15. Under steady-state before $t = 1$ s, the converter operates in *MPPT* mode extracting the maximum power (1 kW under 1000 W/m^2) from the PV panels. The PV voltage is regulated to 138 V, while the inverter dc-side voltage is equal to $v_{dc} = 250$ V, with a duty cycle

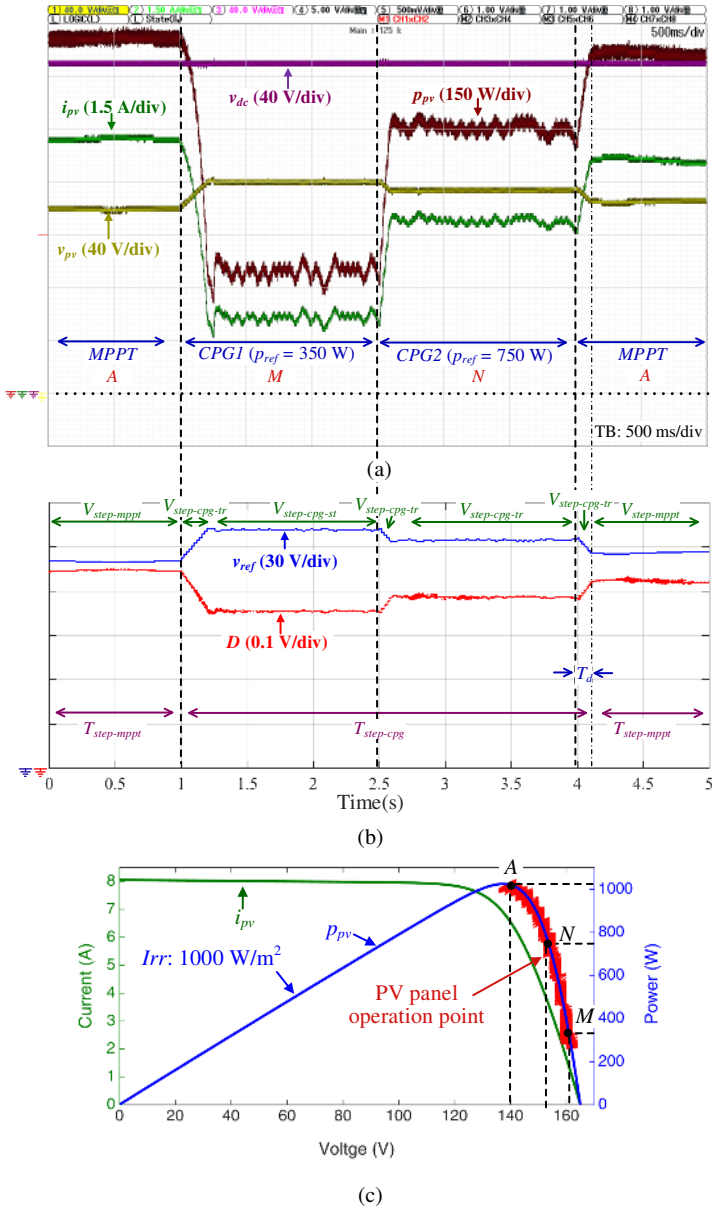

Fig. 15. Experimental results. *Case I* - Behavior of the proposed power reduction method under change of the power reference: (a) PV panel voltage, current, power and dc-link voltage, (b) voltage reference and dc-dc converter duty cycle and (c) PV panel operation point.

of approximately 0.45 and the PV panel operates at Point A of Fig. 15(c).

At $t = 1\,\mathrm{s}$, the external controller sends a direct power reference of $0.35\,\mathrm{kW}$. The calculated voltage reference by the proposed algorithm is $162\,\mathrm{V}$ as shown in Fig. 15(b) and accordingly the operation point moves to Point M in Fig. 15(c). The average value of the extracted power remains $0.35\,\mathrm{kW}$ during this *CPG1* operation mode. At $t = 2.5\,\mathrm{s}$, the power reference changes again to $0.75\,\mathrm{kW}$. During this transient, $V_{step\text{-}cpg}$ is set to $V_{step\text{-}spg\text{-}tr}$ due to the implementation of the proposed hysteresis-band-based controller. Thus, the controllers reaches the new voltage reference quickly and the output power of the converter increases to $0.75\,\mathrm{kW}$ in less than $0.1\,\mathrm{s}$.

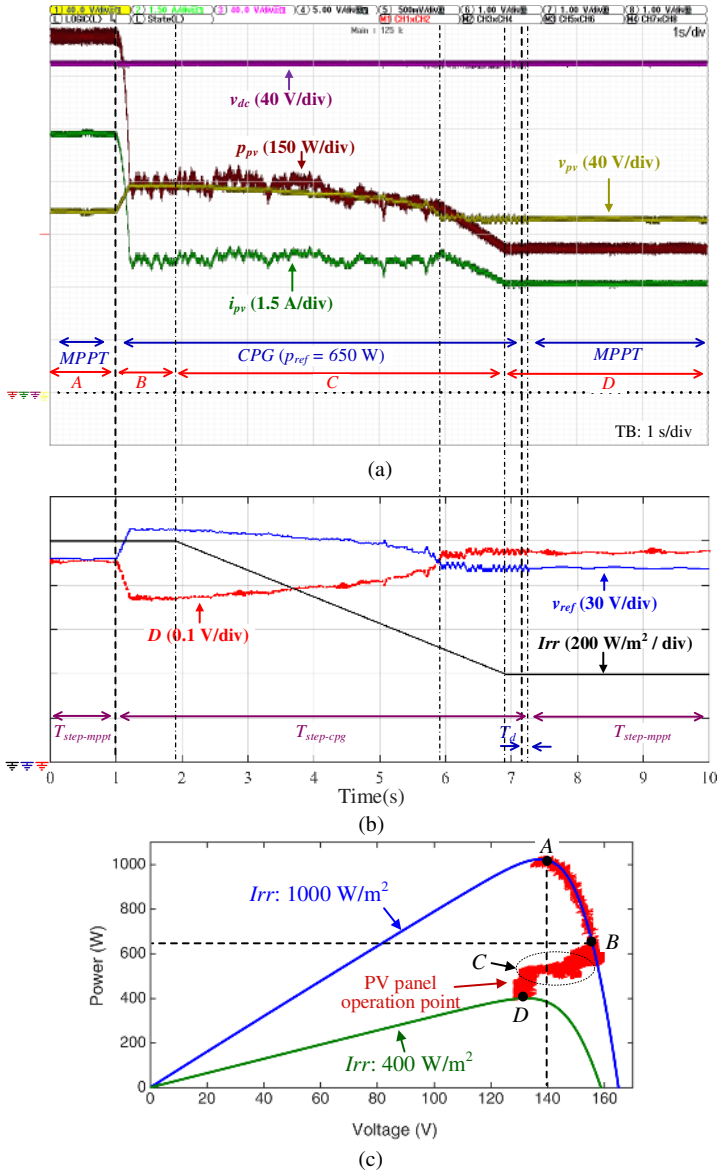

Fig. 16. Experimental results: *Case II* - Behavior of the proposed power reduction method under change of the irradiance: (a) PV panel voltage, current, power and dc-link voltage, (b) voltage reference and dc-dc converter duty cycle and (c) operation point of the PV panel.

The operation mode after $t = 4\,\mathrm{s}$ changes to *MPPT* operation mode, in which the normal P&O algorithm is implemented, the same as the period before $t = 1\,\mathrm{s}$. However, the normal P&O algorithm, with $T_{step\text{-}mppt} = 0.2\,\mathrm{s}$ and $V_{step\text{-}mppt} = 0.5\,\mathrm{V}$ as mentioned in Table II, requires relatively long settling time to calculate v_{mpp} and the results, shown between $t = 4\,\mathrm{s}$ and $t = 5\,\mathrm{s}$, did not reach the steady-state. It can be seen that the proposed controller can quickly regulate the PV panel power to the required power reference, even under a sudden step change of the power reference.

Case II: The second case demonstrates the impact of irradiance to the performance of the proposed algorithm. The irradiance is reduced linearly from $1000\,\mathrm{W/m^2}$ to $400\,\mathrm{W/m^2}$ between $t = 1.95\,\mathrm{s}$ and $t = 6.8\,\mathrm{s}$, while the power

reference is kept constant at $P_{ref} = 0.65\,\mathrm{kW}$. The *CPG* command is received at $t = 1\,\mathrm{s}$ and the controller operates similarly to Case I, at Point *B* in Fig. 16(c). Between $t = 1\,\mathrm{s}$ and $t = 1.95\,\mathrm{s}$, the irradiance is constant $1000\,\mathrm{W/m^2}$, and the PV power is also kept constant. However, after $t = 1.95\,\mathrm{s}$ due to the reduction of the irradiance, V_{ref} changes in order to regulate the power to the requested reference. This happens until $t = 5.9\,\mathrm{s}$. At this moment, the maximum available power from the PV panel is equal to $0.65\,\mathrm{kW}$ and the operating point corresponds to the *MPP*. Further reduction in the irradiance below $595\,\mathrm{W/m^2}$ means that the reference power cannot be satisfied, at which point the algorithm tracks the *MPP*. After $t = 6.9\,\mathrm{s}$, when the irradiance stays constant to $400\,\mathrm{W/m^2}$, the proposed *CPG* algorithm regulates the reference voltage at 132 V, which is equal to the v_{mpp}, as shown in Fig. 16(c) with the PV panel operating at Point *C*. The robustness of the the proposed *CPG* control algorithm is show in this case study and it is demonstrated that it is able to regulate the PV panel power to the required power reference under the change of irradiance.

The cases that are presented and experimentally verified, demonstrate that the proposed algorithm combined with the change in the time- and voltage-step is capable of either controlling the extracted PV power to the required power reference or tracking the maximum power point when the power requirements cannot be satisfied.

VI. Conclusion

A general algorithm for calculating the voltage reference of a PV panel, which regulates its output power to a certain power reference has been introduced and investigated in this paper. The proposed algorithm is based on the P-V curve characteristics of the PV panel. Unlike the presented studies in the literature, the proposed algorithm is flexible in moving the operation point to the right- or left-side of maximum power point and can be applied for single- or two-stage PVPP topologies. As the time- and voltage-step of the voltage reference calculation algorithm are calculated based on a hysteresis band controller, fast dynamic performance during transients and slow power oscillations during steady-state are obtained.

Detailed implementation of the proposed *CPG* algorithm has been presented and its flexibility and effectiveness has been demonstrated on 50-kVA single- and two-stage PVPP simulation setups and a 1-kVA experimental setup, under various irradiance and power reference profiles. The PVPP obtains *CPG* capability under all of the presented severe operating conditions. Also, it is shown that if the target power reference is larger than the maximum available power of the PVPP, the proposed algorithm operates at maximum power point. Furthermore, the robustness of the proposed algorithm for regulating the PVPP power while its operation point goes beyond the open-circuit voltage of the PV panel due to sudden decrease of irradiance, is demonstrated with results for both PVPP topologies. The results demonstrate flexibility and generality of the proposed algorithm as an additional function for existing *MPPT* algorithms in grid-connected PVPPs.

References

[1] S. Sajadian and R. Ahmadi, "Model predictive-based maximum power point tracking for grid-tied photovoltaic applications using a Z-source inverter," *IEEE Trans. Power Electron.*, vol. 31, no. 11, pp. 7611–7620, Nov. 2016.

[2] Y. T. Jeon, H. Lee, K. A. Kim, and J. H. Park, "Least power point tracking method for photovoltaic differential power processing systems," *IEEE Trans. Power Electron.*, vol. 32, no. 3, pp. 1941–1951, Mar. 2017.

[3] S. M. R. Tousi, M. H. Moradi, N. S. Basir, and M. Nemati, "A function-based maximum power point tracking method for photovoltaic systems," *IEEE Trans. Power Electron.*, vol. 31, no. 3, pp. 2120–2128, Mar. 2016.

[4] J. H. Teng, W. H. Huang, T. A. Hsu, and C. Y. Wang, "Novel and fast maximum power point tracking for photovoltaic generation," *IEEE Trans. Ind. Electron.*, no. 99, Apr. 2016.

[5] M. A. Ghasemi, H. M. Forushani, and M. Parniani, "Partial shading detection and smooth maximum power point tracking of PV arrays under PSC," *IEEE Trans. Power Electron.*, vol. 31, no. 9, pp. 6281–6292, Sep. 2016.

[6] H. Renaudineau, F. Donatantonio, J. Fontchastagner, G. Petrone, G. Spagnuolo, J. P. Martin, and S. Pierfederici, "A PSO-based global MPPT technique for distributed PV power generation," *IEEE Trans. Ind. Electron.*, vol. 62, no. 2, pp. 1047–1058, Feb. 2015.

[7] M. Ricco, P. Manganiello, E. Monmasson, G. Petrone, and G. Spagnuolo, "FPGA-based implementation of dual kalman filter for PV MPPT applications," *IEEE Trans. Ind. Informat.*, vol. PP, no. 99, pp. 1–1, 2015.

[8] W. Libo, Z. Zhengming, and L. Jianzheng, "A single-stage three-phase grid-connected photovoltaic system with modified MPPT method and reactive power compensation," *IEEE Trans. Energy Convers.*, vol. 22, no. 4, pp. 881–886, Dec. 2007.

[9] L. R. Chen, C. H. Tsai, Y. L. Lin, and Y. S. Lai, "A biological swarm chasing algorithm for tracking the PV maximum power point," *IEEE Trans. Energy Convers.*, vol. 25, no. 2, pp. 484–493, Jun. 2010.

[10] P. Manganiello, M. Ricco, G. Petrone, E. Monmasson, and G. Spagnuolo, "Optimization of perturbative PV MPPT methods through online system identification," *IEEE Trans. Ind. Electron.*, vol. 61, no. 12, pp. 6812–6821, Dec. 2014.

[11] P. Manganiello, M. Ricco, E. Monmasson, G. Petrone, and G. Spagnuolo, "On-line optimization of the P&O MPPT method by means of the system identification," in *Proc. IEEE Industrial Electronics Conference (IECON)*, Nov. 2013, pp. 1786–1791.

[12] M. Ricco, P. Manganiello, G. Petrone, E. Monmasson, and G. Spagnuolo, "FPGA-based implementation of an adaptive P&O MPPT controller for PV applications," in *Proc. IEEE 23rd Int. Symposium on Industrial Electronics (ISIE)*, Jun. 2014, pp. 1876–1881.

[13] B. Subudhi and R. Pradhan, "A comparative study on maximum power point tracking techniques for photovoltaic power systems," *IEEE Trans. Sustain. Energy*, vol. 4, no. 1, pp. 89–98, Jan. 2013.

[14] K. S. Tey and S. Mekhilef, "Modified incremental conductance algorithm for photovoltaic system under partial shading conditions and load variation," *IEEE Trans. Ind. Electron.*, vol. 61, no. 10, pp. 5384–5392, Oct. 2014.

[15] A. Reinhardt, D. Egarter, G. Konstantinou, and D. Christin, "Worried about privacy? let your PV converter cover your electricity consumption fingerprints," in *Proc. IEEE Inter. Conf. on Smart Grid Communications (SmartGridComm)*, Nov. 2015, pp. 25–30.

[16] D. Sera, L. Mathe, T. Kerekes, S. V. Spataru, and R. Teodorescu, "On the perturb-and-observe and incremental conductance MPPT methods for PV systems," *IEEE J. Photovolts*, vol. 3, no. 3, pp. 1070–1078, Jul. 2013.

[17] M. A. G. de Brito, L. Galotto, L. P. Sampaio, G. D. A. E. Melo, and C. A. Canesin, "Evaluation of the main MPPT techniques for photovoltaic applications," *IEEE Trans. Ind. Electron.*, vol. 60, no. 3, pp. 1156–1167, Mar. 2013.

[18] Y. Yang, H. Wang, F. Blaabjerg, and T. Kerekes, "A hybrid power control concept for PV inverters with reduced thermal loading," *IEEE Trans. Power Electron.*, vol. 29, no. 12, pp. 6271–6275, Dec. 2014.

[19] H. D. Tafti, A. Maswood, G. Konstantinou, J. Pou, K. Kandasamy, Z. Lim, and G. H. P. Ooi, "Study on the low-voltage ride-thorough capability of photovoltaic grid-connected neutral-point-clamped inverters with active/reactive power injection," *IET Renewable Power Generation*, Dec. 2016.

[20] Y. Yang, F. Blaabjerg, and H. Wang, "Constant power generation of photovoltaic systems considering the distributed grid capacity," in *Proc. IEEE Applied Power Electronics Conf. and Exposition (APEC)*, Mar. 2014, pp. 379–385.

[21] A. Urtasun, P. Sanchis, and L. Marroyo, "Limiting the power generated by a photovoltaic system," in *10th Int. Multi-Conferences on Systems, Signals Devices (SSD13)*, Mar. 2013, pp. 1–6.

[22] C. Rosa, D. Vinikov, E. Romero-Cadaval, V. Pires, and J. Martins, "Low-power home PV systems with MPPT and PC control modes," in *Proc. Int. Conf.-Workshop Compatibility And Power Electronics*, Jun. 2013, pp. 58–62.

[23] A. Hoke and D. Maksimovic, "Active power control of photovoltaic power systems," in *Proc. IEEE 1st Conf. on Technologies for Sustainability (SusTech)*, Aug. 2013, pp. 70–77.

[24] R. G. Wandhare and V. Agarwal, "Precise active and reactive power control of the PV-DGS integrated with weak grid to increase PV penetration," in *Proc. IEEE 40th Photovoltaic Specialist Conf. (PVSC)*, Jun. 2014, pp. 3150–3155.

[25] C. Y. Tang, Y. T. Chen, and Y. M. Chen, "PV power system with multi-mode operation and low-voltage ride-through capability," *IEEE Trans. Ind. Electron.*, vol. 62, no. 12, pp. 7524–7533, Dec. 2015.

[26] M. Mirhosseini, J. Pou, and V. G. Agelidis, "Single- and two-stage inverter-based grid-connected photovoltaic power plants with ride-through capability under grid faults," *IEEE Trans. Sustain. Energy*, vol. 6, no. 3, pp. 1150–1159, Jul. 2015.

[27] H. D. Tafti, A. I. Maswood, Z. Lim, G. H. P. Ooi, and P. H. Raj, "NPC photovoltaic grid-connected inverter with ride-through capability under grid faults," in *Proc. IEEE 11th International Conference on Power Electronics and Drive Systems*, Jun. 2015, pp. 518–523.

[28] A. Sangwongwanich, Y. Yang, F. Blaabjerg, and H. Wang, "Benchmarking of constant power generation strategies for single-phase grid-connected photovoltaic systems," in *Proc. IEEE Applied Power Electronics Conf. and Exposition (APEC)*, Mar. 2016, pp. 370–377.

[29] A. Sangwongwanich, Y. Yang, and F. Blaabjerg, "High-performance constant power generation in grid-connected pv systems," *IEEE Trans. Power Electron.*, vol. 31, no. 3, pp. 1822–1825, Mar. 2016.

[30] A. Sangwongwanich, Y. Yang, and F. Blaabjerg, "A sensorless power reserve control strategy for two-stage grid-connected PV systems," *IEEE Trans. Power Electron.*, no. 99, pp. 1–1, Jan. 2017.

[31] J. H. Teng, W. H. Huang, T. A. Hsu, and C. Y. Wang, "Novel and fast maximum power point tracking for photovoltaic generation," *IEEE Trans. Ind. Electron.*, vol. 63, no. 8, pp. 4955–4966, Aug. 2016.

[32] P. Manganiello, M. Ricco, G. Petrone, E. Monmasson, and G. Spagnuolo, "Optimization of perturbative PV MPPT methods through online system identification," *IEEE Trans. Ind. Electron.*, vol. 61, no. 12, pp. 6812–6821, Dec. 2014.

[33] Y. Jiang, J. A. A. Qahouq, and T. A. Haskew, "Adaptive step size with adaptive-perturbation-frequency digital MPPT controller for a single-sensor photovoltaic solar system," *IEEE Trans. Power Electron.*, vol. 28, no. 7, pp. 3195–3205, Jul. 2013.

[34] C. C. Hua, W. T. Chen, and Y. H. Fang, "A hybrid MPPT with adaptive step-size based on single sensor for photovoltaic systems," in *Proc. Intern. Conf. Information Science, Electron. and Electrical Engineering*, vol. 1, Apr. 2014, pp. 441–445.